Thermally-tunable cavity resonator-integrated guided-mode resonance filters

Stéphane Calvez, Antoine Monmayrant, Olivier Gauthier-Lafaye

Thermally-tunable Cavity Resonator-Integrated Guided-mode Resonance Filters

STEPHANE CALVEZ,[1,*] ANTOINE MONMAYRANT,[1] AND OLIVIER GAUTHIER-LAFAYE[1]

[1]LAAS-CNRS, Université de Toulouse, CNRS, 7 avenue du colonel Roche, F-31400 Toulouse, France

**scalvez@laas.fr*

Abstract: We report the fabrication of Cavity Resonator-Integrated Guided-mode Resonance Filters (CRIGFs) using a hybrid lithium-niobate/silicon oxynitride technological platform that allows the exploitation of lithium niobate advantageous material properties while maintaining standard nanoprocessing techniques. The beneficial use of this approach is illustrated with the first demonstration of thermal tuning of a CRIGF.

1. Introduction

Cavity Resonator-Integrated Guided-mode Resonance Filters (CRIGFs) are waveguide Fabry-Perot micro-cavities with an intra-cavity out-of-plane input/output grating coupler whose design corresponds to a Guided-Mode Resonance Filter (GMRF) of finite size [1–4] (see Fig. 1). As such, the overall device operating principle is ruled by the excitation of and emission from supported localized Fabry-Perot modes [3]. The response is thus a fixed-wavelength(s) passband filter in reflection (and a notch filter in transmission) whose peak reflectivity and angular dependence are governed by the overlap between the excitation signal and the localized modes spatial and spectral properties. The resulting reflective characteristics and tolerances [2] make them attractive for use as wavelength-selective mirrors in extended-cavity diode lasers (ECDLs) [5–7]. However, when it comes to introducing tunability into CRIGFs (and associated

ECDLs), the above-mentioned operating principle renders ineffective the use of angular tuning as commonly implemented with other (diffractive, volume Bragg or GMRFs) grating-based approaches. The only viable solutions therefore consist in altering the CRIGF micro-cavity physiccal properties either via its geometry or its constitutive set of refractive indices. To that extent, CRIGFs with spatially-graded grating structures have been successfully demonstrated [8] and used to introduce broadband tuning of ECDLs [9]. Nevertheless, to gain in laser stability and packaged module compactness, it is desirable to devise, demonstrate and implement systems exploiting displacement-free tunable filters. In that context, it is worth noting that GMRFs with suitable tuning mechanisms including electro-refractive [10–12], optofluidic [13] and thermal [14] actuation schemes have already been reported and could readily be transferred to CRIGFs with the preference being given to all-solid approaches.

In this paper, we report the demonstration of thermally-tunable, and therefore movement-free, Cavity Resonator-Integrated Guided-mode Resonance Filters based on a hybrid lithium-niobate (LN)/silicon oxynitride (SiON) platform, the latter being selected as it combines convenient nano-processing afforded by the SiON technology with the ability to exploit the favorable properties of a hard-to-process material : lithium niobate.

2. Design

To demonstrate movement-free tuning of a CRIGF resonance, we selected the lithium niobate on insulator technology as this material platform is compatible with the fabrication of low-loss integrated optics [15,16] and provides various electronic means to modify the material refractive index, namely using either thermal, electro-optic, piezo-electric or even acousto-optic effects [15,16]. More specifically, as summarized in Table 1, $LiNbO_3$ is an attractive material to use to make thermally-active filters as both its refractive index thermal coefficient and its expansion coefficient are greater than the ones of the materials typically used so far (Si_3N_4 for the waveguide core and of AF32 glass ($\alpha=3.2\cdot10^{-6}$ K^{-1}) for the transparent substrate).

Although the CRIGFs could be made by direct corrugation of the waveguide $LiNbO_3$ core, we opted for the hybrid SiON/LN embodiment represented on Fig. 1 since, as detailed below, this approach not only offers an easier processing route [16,17] but also a greater design flexibility thanks to a higher number of optimization parameters.

The CRIGFs were designed for operation at a wavelength of 1550 nm using a combination of rigorous coupled-wave analysis [18] and coupled-mode theory [3]. More specifically, the ~~vertical~~ planar waveguide is constituted of a 297-nm-thick X-cut $LiNbO_3$ core surrounded by a 2 µm SiO_2 under-cladding layer and an upper-cladding bilayer made of a 72 nm Si_3N_4 layer surmounted by 323 nm of silica. The upperclad bilayer allows to optimize the grating effective index difference (i.e. the grating coupling strength) and the overall stack reflectivity. These thicknesses were chosen first and foremost to ensure low-loss TE-polarized (s-polarized) singlemode propagation on an X-cut $LiNbO_3$ substrate with an effective index of 1.821. They also constitute an anti-reflection coating as shown on Fig. 2 right and as calculated using the scattering matrix method [19] with refractive indices taken from references [20,21] and summarized in Table 1.

Table 1. Simulation parameters [20,21]

Material	n	dn/dT (10^{-5} K^{-1})	α (10^{-6} K^{-1})
SiO_2	1.444	0.95	0.55
Si_3N_4	1.979	2.45	2.0
$LiNbO_3$	2.138	3.84	15.4

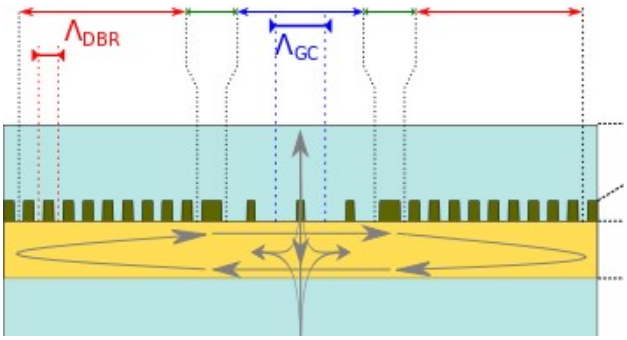

Fig. 1. Diagram of the considered CRIGF structure. The arrows give a schematic representation of the device operating principle where an incident beam (coming from the top) is coupled to localized resonating mode which is out-coupled to form the reflection/transmission response.

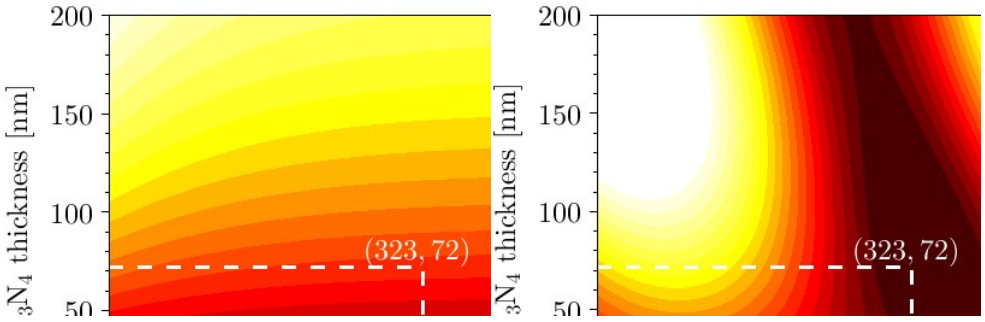

Fig. 2. Grating effective index difference (left) and out of resonance reflectivity (right) at a wavelength of 1550 nm as a function of the two top layers of the structure. Selected thicknesses of the upperclad bilayer (white dashes) minimize the reflectivity.

Assuming that the Si_3N_4 layer is fully etched in the Distributed Bragg Reflectors (DBRs) that establish the CRIGF cavity, the effective index difference between the etched (without the Si_3N_4 layer, of effective index n_1) and unetched (with the Si_3N_4 layer, of effective index n_2) sections of the DBR and GC was evaluated to be 0.0451 (see Fig. 2. left). Using the below-mentioned (thin-film approximation) formulae [22], DBRs with N_p=400-pair and a filling-factor of 0.5 and a period of 432.5 nm exhibit a modal reflectivity, R_{DBR}, at a wavelength of

λ=1550 nm greater than 99.9% with a full-width-at-half-maximum (FWHM) stopband Δλ of ~25.4 nm and thereby support highly-confined localized modes.

$$R_{DBR} = \frac{n_1 n_2^{2N_p} - n_1 n_1^{2N_p}}{n_1 n_2^{2N_p} + n_1 n_1^{2N_p}} \quad (1)$$

$$\Delta\lambda = \frac{4\lambda}{\pi} \operatorname{asin}\left(\frac{|n_2 - n_1|}{n_2 + n_1}\right) \quad (2)$$

Finally, we chose a 21-period grating coupler with a grating pitch of Λ_{GC}=865 nm and a fill-factor of 0.45 as well as phase-adjustment sections of L_{PS}=1.125 Λ_{GC}. With these parameters, the passband reflective filter response sitting an anti-reflective background is predicted to have a FWHM bandwidth of ~0.85 nm with, at resonance, a maximal reflectivity of 85.3% and a minimal transmission of 14.4% as shown in Fig. 3. We note that the remaining 0.3% loss correspond to waveguide losses at the end of the DBRs. Additionally, the spectral range of ripple-free transmission around the resonant wavelength corresponds to the above-mentioned ~25-nm-wide DBR stopband.

Finally, using the thermo-optical coefficients of references [20,21] and assuming that the grating structure expansion is imposed by the substrate, RCWA calculations suggest that the resonant peak will linearly shift at a rate of 0.0476 nm/K with temperature, 43 % of which being due to the substrate thermal expansion. Similarly, the wavelength of the antireflection coating minimum (~1535 nm) is found to increase linearly at a rate of 0.0452 nm/K.

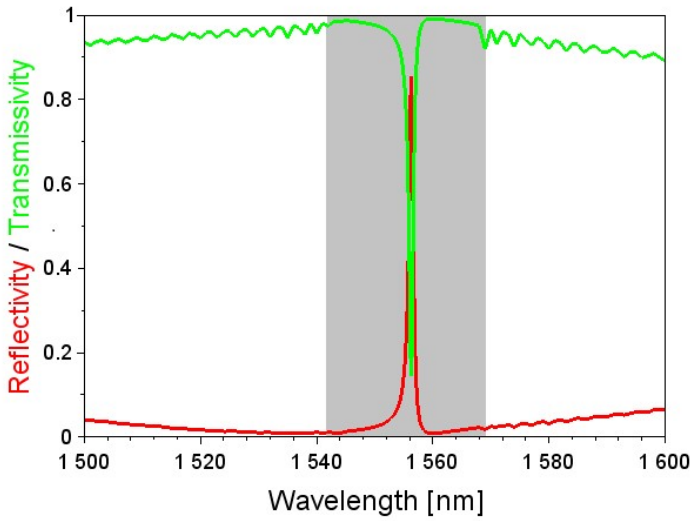

Fig. 3. CRIGF spectral characteristics (reflection in red and transmission in green) as calculated by RCWA (using 901 orders and a mode-matched Gaussian beam [23]). The grey area highlights the DBR stopband.

3. Fabrication

The device fabrication started from a Lithium-Niobate On Insulator (LNOI) planar underclad core waveguide on its substrate obtained from NanoLN. The 72-nm-thick Si_3N_4 layer constituting the first layer of the waveguide upper-cladding was deposited using an Inductive-Coupled-Plasma Plasma-Enhanced Chemical Vapor Deposition (ICP-PECVD) system with single-wavelength (532 nm) in-situ reflectivity control. The designed grating structures were then defined into the latter layer using nano-imprint lithography and dry etching with the 50-µm-long grating lines oriented along the $LiNbO_3$ crystallographic Z-axis (extraordinary axis). As in [24], a master was patterned on a silicon substrate using electron-beam lithography, then replicated into a soft mold by thermal nano-imprint lithography and finally transferred by UV nano-imprint lithography from the soft mold into the resist spun on the LNOI sample. In this last step, the soft mold was peeled off along the grating lines. The grating patterns were then transferred into the Si_3N_4 layer using a CHF_3/O_2-etch with the $LiNbO_3$ top surface serving as

an etch-stop interface given this material chemical inertness and hardness. As a consequence and as shown in Fig. 4, it became easier to control the grating height (and coupling strength) despite the potential presence of a residual resist layer [25]. It also helped obtain smooth surfaces inside the grating trenches (with a measured roughness of 0.6 nm as compared to 3.2 nm at the top of the SiN layer) and therefore high-quality-factor devices by minimizing the roughness-induced limit of the DBR effective reflectivity and of the waveguide propagation loss.

Fig. 4. Atomic-Force Microscope measurement of the profile of the etched grating into the SiN layer.

The device fabrication was completed by ICP-PECVD deposition of a 323-nm-thick SiO_2 layer on top of the above-described grating structure and of a 266-nm-thick SiO_2 single-layer anti-reflective coating on the rear-side of the substrate to avoid back-reflection from the latter interface.

4. Characterization

The device spectral characteristics around a wavelength of 1550 nm were measured using the setup shown in Fig. 5. The data were acquired with a 10-pm resolution using a fiber-coupled tunable laser whose output was relayed using free-space optics to form a beam whose waist was measured to be 5.3-µm. The camera and 850 nm LED illumination were used to image the sample and the 980 nm laser beam served to transversally locate the sample with respect to the probe beam, making use of the collinearity between the 980 and 1550 nm beams. This arrangement is essentially a substitute to using an InGaAs camera to directly monitor the

1550 nm beam. The sample was then longitudinally positioned at the waist by maximizing the reflected signal from an adjacent grating-free area. The transmission and reflectivity responses were respectively calibrated against sample-free transmission and the reflection from a silver mirror. The sample was mounted using silver paste on an aluminum mount presenting a drilled 8mm-diameter via-hole to permit the transmission measurements and whose temperature was measured using a calibrated NTC thermistor and controlled by a thermo-electric Peltier cooler.

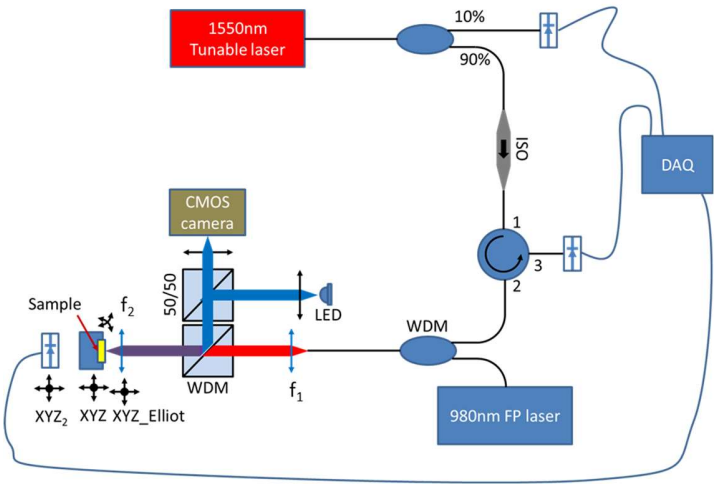

Fig. 5. Characterization setup. The free-space relay is made of the f_1 and f_2-focal-length lens telescope. WDM are wavelength-division multiplexer (spectrally-selective beam splitters). DAQ is a A/N data acquisition card.

As it can be observed on top part of Fig. 6, for a substrate temperature of 20°C, the responses are composed of an antireflective background centered at 1535 nm with a resonant feature observed at ~1554.4 nm with a 0.96-nm linewidth (or equivalently a Q-factor of ~1620) and an on-resonance transmission factor and peak reflectivity of 32±2%. The latter values differ from the calculated ones. These discrepancies are tentatively attributed to residual material and roughness-induced loss contributions (which are not included in the calculations) and to the mode mismatch between the fiber beam profile and the excited CRIGF mode profile.

Furthermore, the observable out-of-resonance ripples are in part due to the DBR structure (as shown in Fig. 3), to the coated substrate Fabry-Perot fringes (that were not included in the calculations) and to spurious transmission fringes resulting from the sensitivity of the fiber part of the measurement setup to the environmental conditions (which primarily affect the device transmissivity).

To gain further insight into the characteristics of the device, the reflectivity was mapped as a function of the position along the grating lines with a slightly offset injection (with respect to the center of the CRIGF (y=0)). As in [3], Fig. 6.bottom reveals, on top of the substrate Fabry-Perot fringe pattern (with ~1-nm free spectral range), a multimode response i.e. a response with several reflectivity peaks. However, contrary to [3], this spectro-spatial map is asymmetric (see Fig. 6 bottom), a feature whose origin is attributed to the lateral unmolding steps performed during the nano-imprint lithography stage. The observed ~0.014-nm/µm resonance spatial gradient leads, here, to an 0.7-nm spectral shift over the entire grating width. It also causes a negligible spectral broadening of the measured response over the sampling beam profile. Indeed, the measured bandwidth is close to the calculated one (Q~1830 - see Fig. 3). Should the targeted Q-factor exceed 16000 [8], an improvement in spatial inhomogeneity would be required.

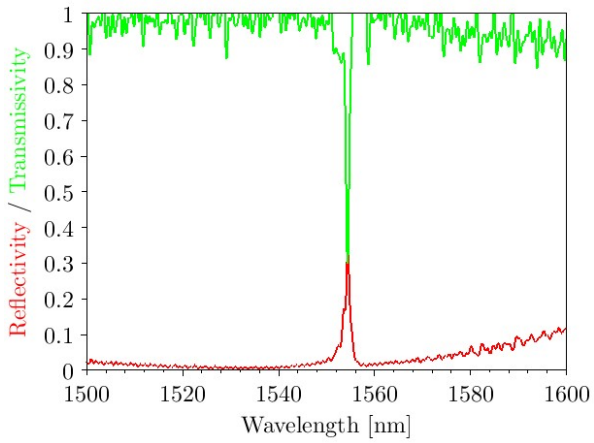

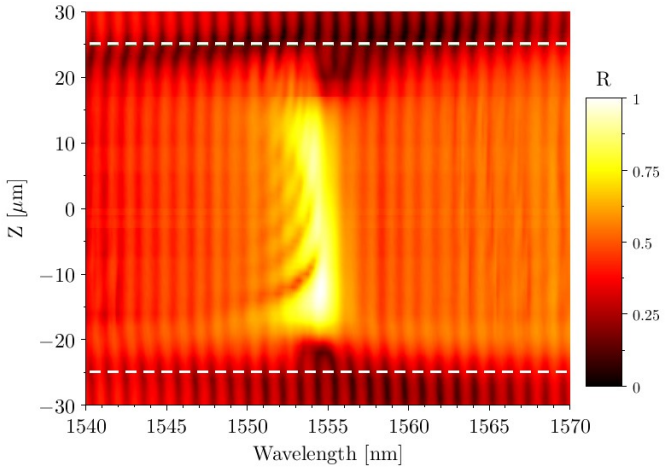

Fig. 6. Top: Typical spectral characteristics at 20°C of the fabricated LNOI CRIGF. Bottom: Spatial dependence of the reflectivity (at 20°C) along the CRIGF grating lines (Z-axis). The white dashed lines show the limit of the CRIGF

Finally, for a fixed sample position, when varying the sample mount temperature from 20 to 80°C, the resonance is shown to shift over a 2.31-nm span, a range ~2.4-time the filter bandwidth (see Fig. 7). The resonance-shifting rate is evaluated to be 0.0382±0.0008 nm/K. Parabolic fits of the anti-reflection coating part of the spectra also reveals a linear shift of the AR minimum at a similar rate (0.0367±0.0057nm/K) in keeping with the predicted theoretical behavior. The discrepancy between the experimentally measured and calculated values is assigned to the difference between the actual sample surface temperature and the measured mount temperature.

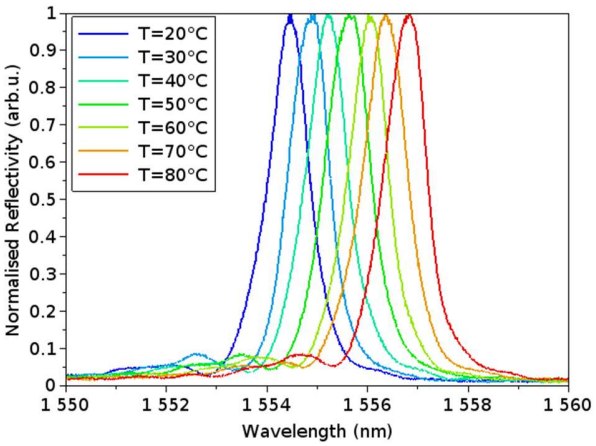

Fig. 7. Temperature dependence of the normalized reflectivity of the fabricated LNOI CRIGF.

5. Conclusion

We reported a thermally-tunable Cavity Resonator-Integrated Guided-mode Resonance Filter exploiting a hybrid lithium-niobate/silicon oxynitride technological platform. The device operating around the central wavelength of 1555 nm was shown to exhibit a Q-factor of ~1620 and to be tunable at a rate of 0.0382 nm/K. Spans larger than the filter bandwidth and an order of magnitude larger than the typical mode spacing of practical extended-cavity diode lasers [5–7,9] were also shown to be achievable upon application of a reasonable temperature rise (>25°C). Future work will include investigations of such electronically-tunable CRIGF-based ECDLs for fine tuning of the laser emission wavelength. Additionally, similarly to the work of reference [17], the demonstrated technological approach of combining the established nano-structuration of silicon oxynitride layers with materials which possess interesting properties but are hard-to-process is thought to be an attractive route to confer advanced functionalities or optimum performance to devices. The specific implementation with LNOI was performed as a step towards the exploitation of its nonlinear properties as it will be reported elsewhere.

Funding

ANR Reson

Disclosures

The authors declare no conflicts of interest.

Acknowledgments

The authors would like to thank NanoLN for providing the LNOI sample onto which the device was fabricated and acknowledge technical support from the LAAS-CNRS micro and nanotechnologies platform, member of the French RENATECH network of cleanroom facilities.

References

1. K. Kintaka, T. Majima, J. Inoue, K. Hatanaka, J. Nishii, and S. Ura, "Cavity-resonator-integrated guided-mode resonance filter for aperture miniaturization," Optics express **20**(2), 1444–1449 (2012).
2. X. Buet, E. Daran, D. Belharet, F. Lozes-Dupuy, A. Monmayrant, and O. Gauthier-Lafaye, "High angular tolerance and reflectivity with narrow bandwidth cavity-resonator-integrated guided-mode resonance filter," Optics express **20**(8), 9322–9327 (2012).
3. R. Laberdesque, O. Gauthier-Lafaye, H. Camon, A. Monmayrant, M. Petit, O. Demichel, and B. Cluzel, "High-order modes in cavity-resonator-integrated guided-mode resonance filters (CRIGFs)," J. Opt. Soc. Am. A **32**(11), 1973 (2015).
4. N. Rassem, A.-L. Fehrembach, and E. Popov, "Waveguide mode in the box with an extraordinary flat dispersion curve," J. Opt. Soc. Am. A **32**(3), 420 (2015).

5. X. Buet, A. Guelmami, A. Monmayrant, S. Calvez, C. Tourte, F. Lozes-Dupuy, and O. Gauthier-Lafaye, "Wavelength-stabilised external-cavity laser diode using cavity resonator integrated guided mode filter," Electronics Letters **48**(25), 1619–1621 (2012).
6. A. Monmayrant, L. Ferrières, V. Lecocq, E. Feuillet, S. Denet, O. Gauthier-Lafaye, and B. Faure, "Performances of a Butterfly-packaged External cavity laser diode with CRIGF mirror," in *European Conference on Lasers and Electro-Optics* (2019), p. CB-P.1 MON.
7. A. Monmayrant, S. Augé, S. Gluchko, A.-L. Fehrembach, E. Popov, T. Antoni, S. Pelloquin, A. Arnoult, G. Maisons, and O. Gauthier-Lafaye, "Wavelength stabilized External Cavity Quantum Cascade Lasers using Cavity Resonator Integrated Grating Filters," in *European Conference on Lasers and Electro-Optics* (2019), p. CB-7.4 WED.
8. S. Augé, A. Monmayrant, S. Pelloquin, J. B. Doucet, and O. Gauthier-Lafaye, "Tunable graded cavity resonator integrated grating filters," Optics Express **25**(11), 12415 (2017).
9. O. Gauthier-Lafaye, S. Augé, X. Buet, and A. Monmayrant, "Graded CRIGF filters for tunable external cavity lasers," in *Conference on Lasers and Electro-Optics* (OSA, 2016), p. JTh2A.109.
10. A. Sharon, H. G. Weber, H. Engel, D. Rosenblatt, A. A. Friesem, and R. Steingrueber, "Light modulation with resonant grating–waveguide structures," Opt. Lett. **21**(19), 1564 (1996).
11. A. S. P. Chang, K. J. Morton, H. Tan, P. F. Murphy, W. Wu, and S. Y. Chou, "Tunable Liquid Crystal-Resonant Grating Filter Fabricated by Nanoimprint Lithography," IEEE Photon. Technol. Lett. **19**(19), 1457–1459 (2007).
12. T. Katchalski, G. Levy-Yurista, A. A. Friesem, G. Martin, R. Hierle, and J. Zyss, "Light modulation with electro-optic polymer-based resonant grating waveguide structures," Opt. Express **13**(12), 4645 (2005).
13. G. Xiao, Q. Zhu, Y. Shen, K. Li, M. Liu, Q. Zhuang, and C. Jin, "A tunable submicro-optofluidic polymer filter based on guided-mode resonance," Nanoscale **7**(8), 3429–3434 (2015).
14. M. J. Uddin and R. Magnusson, "Guided-Mode Resonant Thermo-Optic Tunable Filters," IEEE Photon. Technol. Lett. **25**(15), 1412–1415 (2013).
15. G. Poberaj, H. Hu, W. Sohler, and P. Günter, "Lithium niobate on insulator (LNOI) for micro-photonic devices," Laser & Photonics Reviews **6**(4), 488–503 (2012).
16. A. Boes, B. Corcoran, L. Chang, J. Bowers, and A. Mitchell, "Status and Potential of Lithium Niobate on Insulator (LNOI) for Photonic Integrated Circuits," Laser & Photonics Reviews **12**(4), 1700256 (2018).
17. L. Chang, M. H. P. Pfeiffer, N. Volet, M. Zervas, J. D. Peters, C. L. Manganelli, E. J. Stanton, Y. Li, T. J. Kippenberg, and J. E. Bowers, "Heterogeneous integration of lithium niobate and silicon nitride waveguides for wafer-scale photonic integrated circuits on silicon," Opt. Lett. **42**(4), 803 (2017).

18. P. C. Chaumet, G. Demésy, O. Gauthier-Lafaye, A. Sentenac, E. Popov, and A.-L. Fehrembach, "Electromagnetic modeling of large subwavelength-patterned highly resonant structures," Opt. Lett. **41**(10), 2358 (2016).

19. L. A. Coldren and S. W. Corzine, *Diode Lasers and Photonic Integrated Circuits*, Wiley Series in Microwave and Optical Engineering (Wiley, 1995).

20. L. Moretti, M. Iodice, F. G. Della Corte, and I. Rendina, "Temperature dependence of the thermo-optic coefficient of lithium niobate, from 300 to 515 K in the visible and infrared regions," Journal of Applied Physics **98**(3), 036101 (2005).

21. A. Arbabi and L. L. Goddard, "Measurements of the refractive indices and thermo-optic coefficients of Si_3N_4 and SiO_x using microring resonances," Optics Letters **38**(19), 3878 (2013).

22. H. E. Li and K. Iga, eds., *Vertical-Cavity Surface-Emitting Laser Devices*, Springer Series in Photonics No. v. 6 (Springer, 2003).

23. N. Rassem, E. Popov, and A.-L. Fehrembach, "Numerical modeling of long sub-wavelength patterned structures," Opt Quant Electron **47**(9), 3171–3180 (2015).

24. S. Pelloquin, S. Augé, K. Sharshavina, J.-B. Doucet, A. Héliot, H. Camon, A. Monmayrant, and O. Gauthier-Lafaye, "Soft mold NanoImprint Lithography: a versatile tool for sub-wavelength grating applications," Microsystem Technologies 1–8 (2018).

25. C. M. Sotomayor Torres, S. Zankovych, J. Seekamp, A. P. Kam, C. Clavijo Cedeño, T. Hoffmann, J. Ahopelto, F. Reuther, K. Pfeiffer, G. Bleidiessel, G. Gruetzner, M. V. Maximov, and B. Heidari, "Nanoimprint lithography: an alternative nanofabrication approach," Materials Science and Engineering: C **23**(1–2), 23–31 (2003).